IJIE

Journal homepage: http://penerbit.uthm.edu.my/ojs/index.php/ijie
ISSN : 2229-838X e-ISSN : 2600-7916

The International Journal of Integrated Engineering

On the Internal Enrichment Implementation For Non-Convex Paths, Discontinuities and Crack Problems

Ali Tayebi Derazkola[1], Ali Rahmani Firoozjaee[1*], Mehdi Dehestani[1]

[1]Faculty of Civil Engineering, Babol Noshirvani University of Technology, Babol, Postal Box: 484, Postal Code: 47148-71167, I.R. Iran

*Corresponding Author

DOI: https://doi.org/10.30880/ijie.2022.14.04.013
Received 24 December 2020; Accepted 27 August 2021; Available online 20 June 2022

Abstract: Studies on the cracked plates have shown high variations in the stress values around the crack tip. On the other hand, micro-cracks are observed in man-made pieces. Thus, analysis of stress fields as well as displacement at the crack tip will be inevitable and very important. Mesh-free methods are new techniques that do not require applying the communication-based concept on what is presented in the finite element method. The discretization of the problem domain is done by a set of node points. In the present study, the Element-Free Galerkin (EFG) method was used to analyze the problems of linear elastic stress field in cracked bodies. Two important and essential measures (steps) were done for increasing the accuracy of the results obtained from the analysis of the problems. In the first step, the standard moving least squares shape function was enriched for capturing discontinuity, using some extra basis functions obtained from analytical solutions. In the next step, some consideration was applied in the case of confronting non-convex paths and discontinuities. For this purpose, the diffraction method was used to generate suitable shape functions. Finally, the accuracy of the results and proper efficiency of the proposed extended EFG method were assessed by the standard problem analysis and the results of numerical analysis were compared with the theoretical results.

Keywords: Element-Free Galerkin (EFG) Method, Crack Modeling, Enrichment of Basis Functions, Diffraction Technique, Stress Concentration Factor

1. Introduction

Today, the fracture of materials is one of the most important issues in developing the industry. Thus, it is essential to have sufficient information and knowledge about material fractures to prevent sudden fractures and unexpected failures in the structures. Given that, man-made structures always have structural defects such as the existence of fine cracks, it is always helpful to know about the displacement and stress fields around the crack tip. Ensuring the analysis of the cracks is very important to identify and evaluate the safety and to predict the structural stability. Due to the advances in computer science, the use of numerical methods has become popular due to their low cost and good accuracy. One of the recently developed numerical methods is named mesh-free method. These methods mainly approximate the unknown field by a linear combination of shape functions built without requiring the recourse to mesh the domain. In the recent decades, several mesh-free methods have been used for analysis of the engineering problems including the Smoothed Particle Hydrodynamics (SPH) method[1], Element –Free Galerkin (EFG) method[2], Reproducing Kernel Particle (RKP) method[3], Finite Point (FP) method[4], the HP-meshless clouds method[5], Meshless Local Petrov-Galerkin (MLPG) method[6], Local Boundary Integral Equation (LBIE) method[7], finite cloud method[8], and Discrete Least Squares Meshless (DLSM) method[9], [10].

*Corresponding author: rahmani@nit.ac.ir

Numerous numerical methods have been proposed to model the fracture in the last few decades including the Standard Finite Element Method (FEM)[11]–[21], the Extended Finite Element Method (XFEM)[22]–[24], and the Hybrid Finite Element Method[25], [26], that all of them have provided an appropriate level of accuracy. Chan et al., investigated the ability of the FEM to determine the stress concentration factor around the crack tip, taking into account the influence of the dimensions of the element[18]. Melenk and Babuska (1996) attempted to reduce the computational cost and increase the finite element accuracy, and they developed a method called the Partition of Unity Finite Element Method (PUEFM)[27]. In the next few years, a method known as the extended finite element was proposed and developed by other researchers, such as Belytschko and Moes [22], [24], [28]. It should be noted that the XFEM has some drawbacks. In general, the use of mesh-based approaches for analysis of problems with complex or moving boundaries or those changing over time in geometry and topology analysis will require an iterative and continuous problem domain meshing process. Clearly, analysis of such problems is very costly and time-consuming. For addressing such problems, many researchers have focused on the mesh-free methods[28]–[37]. Nayroles et al., introduced a reasonable and acceptable method for analysis of the engineering problems known as the Diffuse Element Method (DEM) [11]. Then, Belystchko developed the EFG method in 1994 based on the DEM[31], [32].

In each method, there are inherent limitations causing problems in the process of problem analysis. At the beginning of applying the mesh-free methods in the 1970s, this method was first used by Gingold and Monaghan as the (SPH method to study and model the astronomical phenomena for simulating the formation of stars. The problem in the mesh-free methods is modeled in its domain and boundaries through the arrangement and placement of a set of nodes in the problem area. It should be noted that, this set of nodes does not represent a mesh, so no relationship will be required between the nodes. Over the past 20 years, the EFG method has been one of the most interesting and popular methods in the field of fracture problems. The EFG approximation for the discrete system has been based entirely on the parameters of the nodal values. In this method, smoothing weight function techniques, enrichment, and nodal refinement in a local sub-domain adjacent to the crack tip have been used to simulate the fracture problems. Belytschko et al., (1995) used the EFG method to study the cracked plates[31].

Thus, they used the concentration and nodal refinement around the crack tip in order to obtain the appropriate results. Fleming et al., (1997) also used the EFG method to analyze the crack problems[28]. They used two enrichment techniques to overcome the stress field singularity called the internal enrichment and external enrichment. So that, the changes made in the first technique were in the approximation function and the second technique was the basis function. In the second enrichment technique within the formulation framework, they enriched part of the problem area in the vicinity of the cracks around the basis function and used the linear function in the rest of the problem areas. Based on this method, they carried out the investigations on the plate with an edge crack subjected to tensile and shear tension. Li and Cheng (2005) used an enriched meshless manifold method for crack modeling[38]. The local enrichment around the crack was used in order to improve the accuracy, finite cover approximation theory was proposed to model the cracks. Muthu et al., (2014) proposed a closed integral technique in order to obtain the stress concentration factor[33]. In this regard, the EFG method was used based on local enrichment of nodes around the crack. They showed that the applied technique has appropriate accuracy. In relation to the fracture problem, Liaghat et al., (2019) used the cohesive crack technique in the numerical method[30].

They used the mesh-free radial point interpolation method for numerical simulation. Visibility criteria were also used to introduce the crack discontinuity. The validity and effectiveness of this method were confirmed by analyzing the problems of cracked structures. Several studies have been performed using artificial neural network modeling approach to investigate stress concentration and crack propagation. This method is inspired from the working of the human brain. An artificial neural network acquires the data during the training process. These data should be obtained from experimental results or mathematical results or numerical methods[39]–[41].

Thus, in the present study, the extended element-free Galerkin (XEFG) method is proposed to solve the fracture problems and study the stress distribution around the crack by linear elastic fracture analysis according to the advantages of mesh-free methods over mesh-based ones. The internal enrichment method is used to increase the accuracy in high gradient areas such as the crack tip for introducing the crack discontinuity. One of the advantages of this method is that the unknown coefficients are not added to the system of equations that results in not imposing high computational costs. Finally, among the available techniques and methods for introducing the crack and its consequence, the calculation of stress concentration factor, diffraction criterion technique, and J-integral method were used due to their simplicity and providing the required accuracy.

2. Moving Least Squares (MLS) Approximation

Around 1960, MLS approximation has been used for smoothing the surface interpolation of the points with variable values, and it is now one of the most widely used methods among the mesh-free methods to approximate the functions. $\phi(\mathbf{x})$ is the function of the field variation in the domain Ω_x, the MLS approximation in the influence domain for any arbitrary point x can be defined as following:

$$U(\mathbf{x}) \cong \varphi(\mathbf{x}_k) = \sum_{k=1}^{n} P_k(\mathbf{x}) a(\mathbf{x}) = P_k^T(\mathbf{x}) a(\mathbf{x}) \qquad \forall x \in \Omega_{\mathbf{x}} \tag{1}$$

Where, n is the total number of the terms in polynomials basis and a(x) represents the coefficients vector, which is a function of x:

$$a^T(\mathbf{x}) = \{a_0(x) \;\; a_1(x) \;\; a_2(x) \;\; ... \;\; a_m(x)\} \tag{2}$$

In Equation (1), P(x) is a basis functions vector that is chosen from the lowest order monomers in most cases. It should be noted that, the increase in the number of basis terms increases the accuracy and access to stress domain with specific characteristics for example, singularity at the crack tip or stress discontinuity in the interface of the two materials. The number of basic terms (m) can be determined for polynomials with the highest order (t) in the following relationships:

$$m = \frac{(t+1)(t+2)}{2} \qquad \text{Two-dimensional domain} \tag{3}$$

$$m = \frac{(t+1)(t+2)(t+3)}{6} \qquad \text{Three-dimensional domain} \tag{4}$$

For example, in the one-dimensional domain, we have:

$$P^T(\mathbf{x}) = \left[1, x, x^2, x^3, ..., x^m\right] \tag{5}$$

In the two-dimensional domain:

$$P^T(\mathbf{x}) = [1, x, y] \qquad \text{Linear basis} \tag{6}$$

$$P^T(\mathbf{x}) = \left[1, x, y, x^2, xy, y^2\right] \qquad \text{Second-order basis} \tag{7}$$

$$P^T(\mathbf{x}) = \left[1, x, y, x^2, xy, y^2, x^3, x^2y, xy^2, y^3\right] \qquad \text{Third-order basis} \tag{8}$$

The coefficients, a(x) can be determined by minimizing a weighted discrete L_2 norm with respect to these coefficients:

$$J = \sum_{I}^{n} \hat{W}(\mathbf{x} - \mathbf{x}_I)\left[U(\mathbf{x} - \mathbf{x}_I) - \varphi(\mathbf{x}_I)\right]^2 = \sum_{\mathrm{I}}^{\mathrm{n}} \hat{\mathrm{W}}(\mathrm{x} - \mathrm{x_I})\left[\mathrm{P^T(x_I)\ a(x) - \varphi_I}\right]^2 \tag{9}$$

Where, $\hat{W}(\mathbf{x} - \mathbf{x}_I)$ is the weight function for node I, which is zero outside of the influence domain of node I. The weight functions have two important roles in creating the shape functions by the MLS method. Firstly, the weight function provides the weight values for the residuals at different nodes in the influence domain. Secondly, it ensures that the nodes leaving or entering the influence domain are formed gradually when X moves. This is of high importance because, in this way, it makes sure that the constructed MLS shape function satisfies the compatibility condition. The minimization condition requires:

$$\frac{\partial J}{\partial a} = 0 \tag{10}$$

Resulting in the linear equation system:

$$\mathrm{A(x)\,a(x)=B(x)\,U} \tag{11}$$

$$A(\mathbf{x})=\sum_{I}^{n}\hat{W}(\mathbf{x}-\mathbf{x}_I)P(\mathbf{x}_I)P^T(\mathbf{x}_I) \tag{12}$$

$$B(\mathbf{x})=\lfloor B_1 \quad B_2 \quad B_3 \ldots B_n \rfloor \tag{13}$$

$$B_I=\hat{W}(\mathbf{x}-\mathbf{x}_I)\,P(\mathbf{x}_I) \tag{14}$$

Where, U_S is the vector collecting the nodal parameters of the field variation for all nodes in the influence domain:

$$U_s=\{U_1,U_2,\ldots,U_n\} \tag{15}$$

So, the coefficients of the vector are determined:

$$a(\mathbf{x})=A^{-1}(\mathbf{x})B(\mathbf{x})U_s \tag{16}$$

Substituting the above equation into Equation 9 gives us the following equation:

$$U(\mathbf{x})=\sum_{I}^{n}\sum_{J}^{m}P_J(\mathbf{x})(A^{-1}(\mathbf{x})B(\mathbf{x}))_{JI}U_I \tag{17}$$

$$U(\mathbf{x})=\sum_{I}^{n}\varphi_I(\mathbf{x})U_I \tag{18}$$

The shape function of the MLS can be presented as follows:

$$\varphi_I(\mathbf{x})=\sum_{j}^{m}P_j(\mathbf{x})(A^{-1}(\mathbf{x})B(\mathbf{x}))_{jI}=P^T A^{-1}B_I \tag{19}$$

3. Enrichment of Basis Functions

In the previous studies, the internal enrichment method has been proposed to increase the approximation accuracy of the analysis results, especially in discontinuity problems such as structures with cracks [42]. This method is based on adding terms to the basis functions to increase the accuracy of the results around the discontinuities with high gradients. Since, the crack is investigated as a cause of discontinuity in this study; therefore, the components of the displacement domain at the crack tip are proposed and adopted as terms added to the basis function. Relations of displacement obtained by theoretical analysis are presented as follows[42]:

$$U_x=\frac{K_I}{2\mu}\sqrt{\frac{r}{2\pi}}Cos\frac{\theta}{2}\left(\kappa-1+2Sin^2\frac{\theta}{2}\right) \tag{20}$$

$$U_y=\frac{K_I}{2\mu}\sqrt{\frac{r}{2\pi}}Sin\frac{\theta}{2}\left(\kappa+1-2Cos^2\frac{\theta}{2}\right) \tag{21}$$

Where, μ and K_I are the shear modulus and the stress concentration factor of the mode I, respectively r denotes the distance from the crack tip, θ is the angle for the line of the crack tip connecting to the line tangent to the crack tip direction according to Fig.1 ,and κ for the plane stress analysis is equal to $\frac{3-\nu}{1+\nu}$, where ν is the Poisson coefficient.

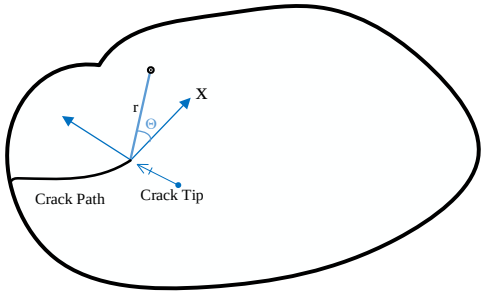

Fig. 1 - Coordinate axes at the crack tip

The basis function was selected in two dimensions for the problem analysis:

$$P^{lin} = \{1, x, y\} \tag{22}$$

According to the relations of displacement of the crack tip, the adopted enrichment components are as follows:

$$\mathrm{P}^{\mathrm{enr}} = \left\{ \sqrt{\mathrm{r}}\sin\frac{\theta}{2}, \sqrt{\mathrm{r}}\cos\frac{\theta}{2}, \sqrt{\mathrm{r}}\sin\theta\sin\frac{\theta}{2}, \sqrt{\mathrm{r}}\sin\theta\cos\frac{\theta}{2} \right\} \tag{23}$$

Therefore, the basis function is generally as follows:

$$P^T(\mathbf{x}) = \left\{ 1, x, y, \sqrt{r}\sin\frac{\theta}{2}, \sqrt{r}\cos\frac{\theta}{2}, \sqrt{r}\sin\theta\sin\frac{\theta}{2}, \sqrt{r}\sin\theta\cos\frac{\theta}{2} \right\} \tag{24}$$

4. Weight Function

In all the mesh-free methods, many weight functions are used to provide the shape functions. The main characteristic of these functions is that they are greater than zero inside the sub-domain and they are zero outside the sub-domain. It should be noted that, the shape functions in some mesh-free methods do not satisfy the Kronecker Delta condition. In this study, the cubic spline weight function was used[43] , which is given as follows:

$$\hat{W}(\mathbf{x}-\mathbf{x}_I) = \overline{W}(\bar{d}) = \begin{cases} \frac{2}{3} - 4\bar{d}^2 + 4\bar{d}^3 & \bar{d} \le \frac{1}{2} \\ \frac{4}{3} - 4\bar{d} + 4\bar{d}^2 - \frac{4}{3}\bar{d}^3 & \frac{1}{2} \le \bar{d} \le 1 \\ 0 & \bar{d} \ge 1 \end{cases} \tag{25}$$

$$\bar{d} = \frac{\left|\mathbf{x}-\mathbf{x}_I\right|}{d_w} = \frac{d}{d_w} \tag{26}$$

Where, $\mathbf{x}$ and $\mathbf{x}_I$ are the coordinates of the Gauss points and nodal, respectively and d_w is the influence domain for a node $\mathbf{x}_I$.

5. The Governing Equations

A two-dimensional, linear elastic problem on the domain Ω was considered as shown in Fig. 2. The governing equilibrium equation is as follows:

$$\nabla.\sigma + b = 0 \qquad \Omega \ Domain \tag{27}$$

Where, σ is the stress vector related to the displacement domain U and b is the force vector.
The boundary conditions will be as follows:

$$\sigma.n = \bar{t} \qquad \text{Based on the stress } \Gamma_t \text{ on the boundary} \tag{28}$$

$$\mathbf{u} = \hat{\mathbf{u}} \qquad \text{Based on the displacement } \Gamma_u \text{ on the boundary} \tag{29}$$

Given the weak form, the final discrete equations will be obtained as follows:

$$K\,U = f \tag{30}$$

$$K_{ij} = \int_{\Omega} B_i^T D\, B_j \, d\Omega - \int_{\Gamma_u} \Phi_i \, SN\, D\, B_j \, d\Gamma - \int_{\Gamma_u} B_i^T \, D^T \, N^T \, S\, \Phi_j \, d\Gamma \tag{31}$$

$$f_i = \int_{\Gamma_t} \Phi_i \, \bar{t} \, d\Gamma + \int_{\Omega} \Phi_i \, b \, d\Omega + \int_{\Gamma_u} B_i^T \, D^T \, N^T \, S\, \bar{U} \, d\Gamma \tag{32}$$

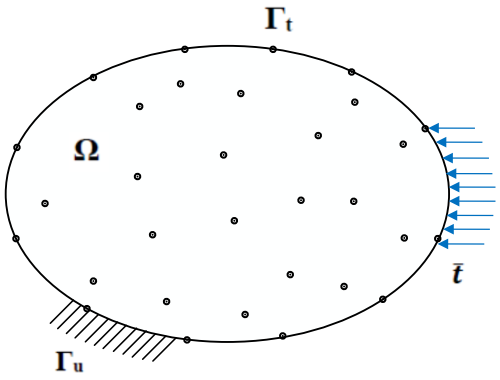

Fig. 2 - Discretization of the problem domain by nodal points, Γ_t derivative boundary conditions, and Γ_u main boundary condition

For plane stress problems, we have:

$$D=\frac{E}{1-\vartheta^2}\begin{bmatrix} 1 & \vartheta & 0 \\ \vartheta & 1 & 0 \\ 0 & 0 & \frac{1-\vartheta}{2} \end{bmatrix} \tag{33}$$

$$B_I=\begin{bmatrix} \Phi_{I,x} & 0 \\ 0 & \Phi_{I,y} \\ \Phi_{I,y} & \Omega_{I,x} \end{bmatrix} \tag{34}$$

$$N=\begin{bmatrix} n_x & 0 & n_y \\ 0 & n_y & n_x \end{bmatrix} \tag{35}$$

$$\mathrm{S}=\begin{bmatrix} \mathrm{S}_x & 0 \\ 0 & \mathrm{S}_y \end{bmatrix} \tag{36}$$

$$S_x=\begin{cases} 1 & \text{If } U_x \text{ is defined on } \Gamma_u \\ 0 & \text{If } U_y \text{ is defined on } \Gamma_u \end{cases}$$

$$S_{y=}\begin{cases} 0 & \text{If } U_x \text{ is defined on } \Gamma_u \\ 1 & \text{If } U_y \text{ is defined on } \Gamma_u \end{cases}$$

Where, E and ϑ are modulus of elasticity and Poisson coefficient, respectively. It should be noted that, the stiffness matrix K is a symmetric matrix.

6. Introducing the Discontinuity in the Mesh-Free Method

Discontinuities in the solid mechanics are classified into two groups: strong discontinuity and weak discontinuity. Strong discontinuity in the displacement field includes the cracks and weak discontinuity involves the discontinuity of the displacement derivatives called as strain discontinuity. Since, the crack is of the discontinuity type in the displacement field thus, it is considered as a strong discontinuity, and the mesh-free method is based on the use of smooth shape function applying the derivatives with high orders of consistency. Therefore, it is important to define the discontinuities in order to solve the crack problems in the mesh-free method. Visibility, diffraction, and transparency criteria are among some methods used for introducing the correct discontinuity. In this study, the diffraction criterion was used to introduce the discontinuity. This method was first introduced and developed by Belytschko et al., to be used in two-dimensional problems. This method was inspired by the diffraction phenomenon of light, and it is based on making the changes in weight values, where the weight function is defined. In this method, the function is deviated and deformed near the crack tip, and the radius of influence around the crack tip is broken and circumvents the crack tip. Therefore, the modified distance in the diffracted zone will be as follows:

$$S(\mathbf{x})=\left(\frac{S_1+S_2(\mathbf{x})}{S_0(\mathbf{x})}\right)^{\lambda} S_0(\mathbf{x}) \tag{37}$$

Where, $S_0(\mathbf{x}) = \left\| \mathbf{x} - \mathbf{x_I} \right\|$ and $S_1(\mathbf{x}) = \left\| \mathbf{x}_T - \mathbf{x}_I \right\|$. X represents the Gauss points, $\mathbf{x}_I$ denotes the nodal points, and $\mathbf{x}_T$ represents the coordinates of the crack tip point (Fig. 3). The parameter λ is most often set to be 1 or 2.

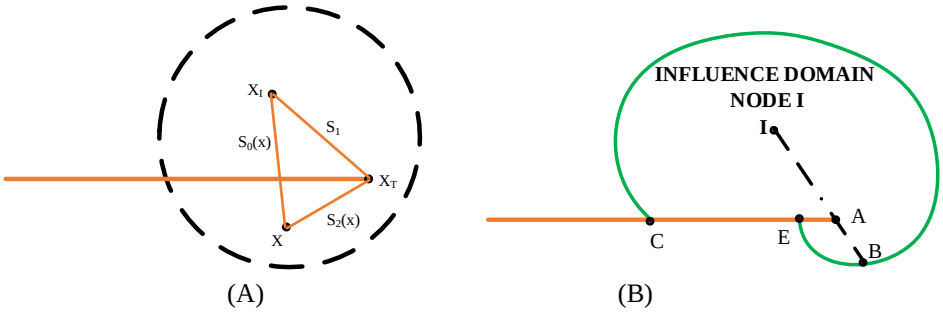

(A) (B)

Fig. 3 - (a) Diffraction method design near the crack tip and (b) Influence domain of node I

7. Numerical Results

Analyses were performed on the plates with edge crack, double crack, and central crack to investigate the performance and accuracy of the results obtained by the extended element-free Galerkin method, around the crack, and near the crack tip. The governing theory suggests the linear elastic stress domain in the cracked body and the relations used in this analysis are based on the plane stress. Elasticity coefficient of $E = 3 \times 10^7 \, Mpa$ and Poisson coefficient of $\nu = 0.3$ were chosen for all the problems. According to the theory, the solution to the stress concentration factor can be obtained as follows:

$$K_I = C\sigma\sqrt{\pi a} \tag{38}$$

Where, a is the crack length, σ represents the applied stress, and C is the correction coefficient, which can be calculated for the different modes of crack displacement in the plate. In the numerical analysis of the cracked plates, the J integral method was used to compute the K_I. For evaluating the results, the error value is given by the following relation:

$$Error = \frac{\left| (K_I)_{XEFG} - (K_I)_{exact} \right|}{(K_I)_{exact}} \times 100 \tag{39}$$

All simulations are performed on hp Intel(R) Core (TM) i7-6700HQ CPU @2.60 GHz and 16 GB RAM.

7.1 Edge -Cracked Plate

As shown in Fig. 4(a'), a rectangular plate was investigated with dimensions of 1×2 m and an edge crack subjected to the tensile stress of $\sigma = 1^{Mpa}$ and shear stress of $\tau = 0^{Mpa}$ in the lower and upper edges. This plate was analyzed for the node numbers of 233, 499, and 865 with regular node arrangement as depicted in Fig. 4(b), as well as a number of different Gauss points. The correction factor C for calculation of the K_I is determined by the following relation:

$$C = 1.12 - 0.231(a/W) + 10.55(a/W)^2 - 21.72(a/W)^3 + 30.39(a/W)^4 \tag{43}$$

As demonstrated in Fig. 5, the results of the stress domain showed that the singular stress is captured by regular XEFG and the effects of crack discontinuity are clearly visible. As indicated in Fig.6, the stress distribution ahead of the crack was in good agreement with the theoretical results and the effects of enrichment on the crack tip and stress values were observed so that, the results related to the lack of enrichment showed more stress in the vicinity of the crack tip according to introducing of the crack but it was unacceptable in comparison with the theoretical results.

However, the effects of the number of Gauss points were evident with respect to the value stress at the crack tip, especially on the node number of 865(Fig. 7).

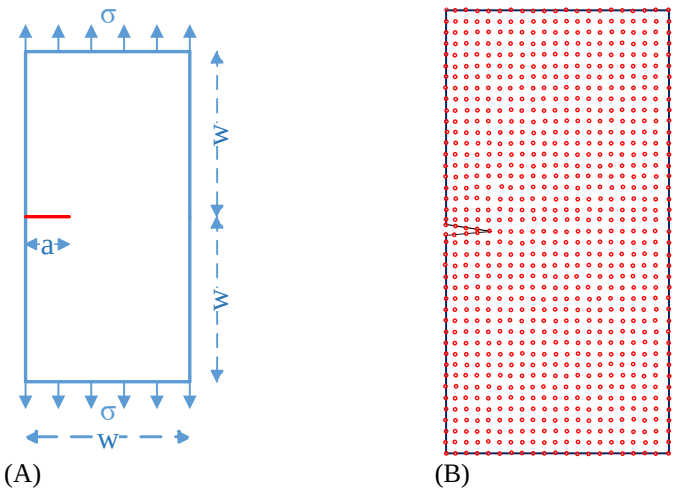

Fig. 4 - (a) Plate with an edge crack subjected to uniform tension; (b) Node arrangement

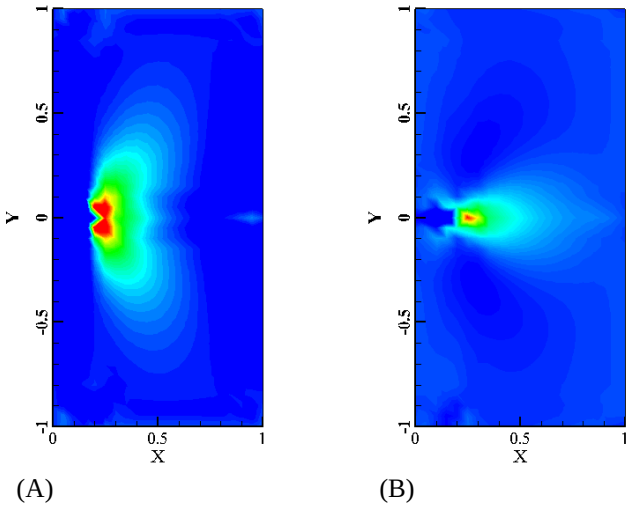

Fig. 5 - Stress contour for 865 nodes and 7850 Gauss points (a) In the Y direction; (b) In the X direction

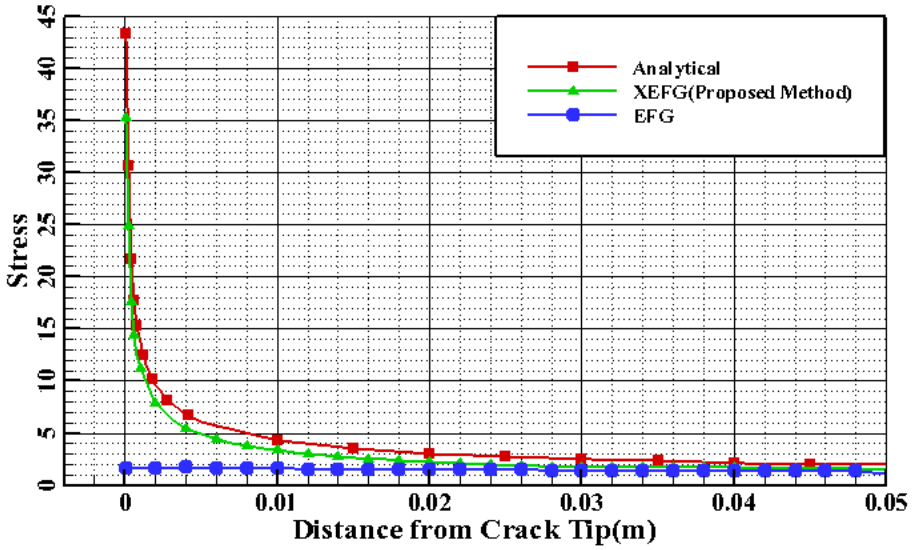

Fig. 6 - Comparison of stress variations along the crack tip for XEFG, EFG, and Analytical methods

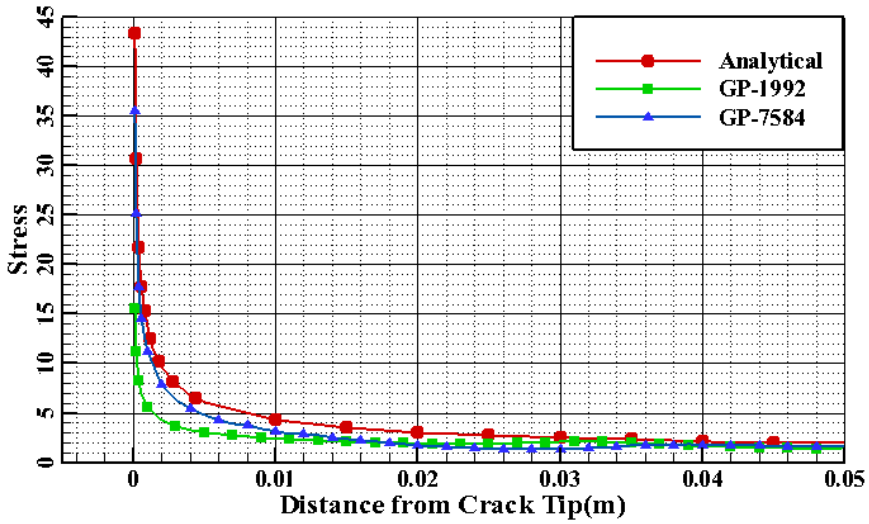

Fig. 7 - The variation in stress along the crack tip for 865 nodes and different numbers of Gauss points

Table 1 shows K_I values and error values obtained based on relation (42). The results of K_I values showed that they were satisfactory for the node numbers of 865 and 499 but they were not acceptable for the node number of 233. It should be noted that, the K_I results were incorrect and could not be verified in the non-enriched state for the node numbers equal to the enriched state.

Table 1 - K_I and error values obtained relative to analytical values

865		499		233		
Error	**$K_{I\text{-}XEFG}$**	**Error**	**$K_{I\text{-}XEFG}$**	**Error**	**$K_{I\text{-}XEFG}$**	
2.38	1.06074	2.41	1.06036	-	-	7584
0.84	1.0775	3.81	1.128	94.6	2.115	5320
-	13.96	-	13.31	203.5	3.298	1992

a. Double-Edge Cracked Plate

In this section, a plate with dimensions of 2×2 m with a double-sided edge crack of 0.2 m is considered for simulations as shown in Fig.8 (a). For the symmetry shown in Fig. 8(b), a second plate under tensile stress of $\sigma = 1^{Mpa}$ and shear stress of $\tau = 0^{Mpa}$ in the lower and upper regions was analyzed with regular nodal arrangement. The correction factor C for calculation of the K_I is obtained as follows:

$$C = 1.12 + 0.20(a/W) - 1.20(a/W)^2 + 1.93(a/W)^3 \quad (41)$$

Studying the stress results along the crack axis showed that it has good accuracy compared to the theoretical values (Figs.9 and 10). It should be noted that, according to the results obtained from analysis of the double -cracked plate, the stress singularity around the crack tip is captured under both enrichment and non-enrichment conditions, guaranteeing the suitability of the adopted method and the enrichment effects are evident on the stress values. Fig.11 shows the variation of K_I values with respect to the number of Gauss points so that, the effects of choosing the number of Gauss points are evident on the accuracy of K_I values**.** Studying the K_I values showed that they were satisfactory for the node numbers of 865 and 499.

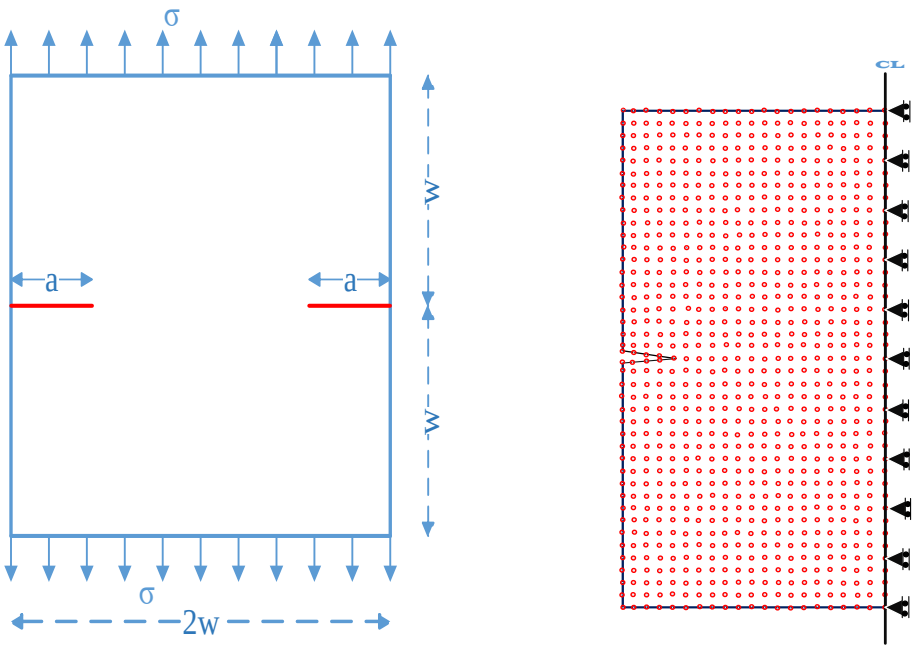

(A) (B)

Fig. 8 - (a) Plate with double cracks under tensile stress (b) Node arrangement

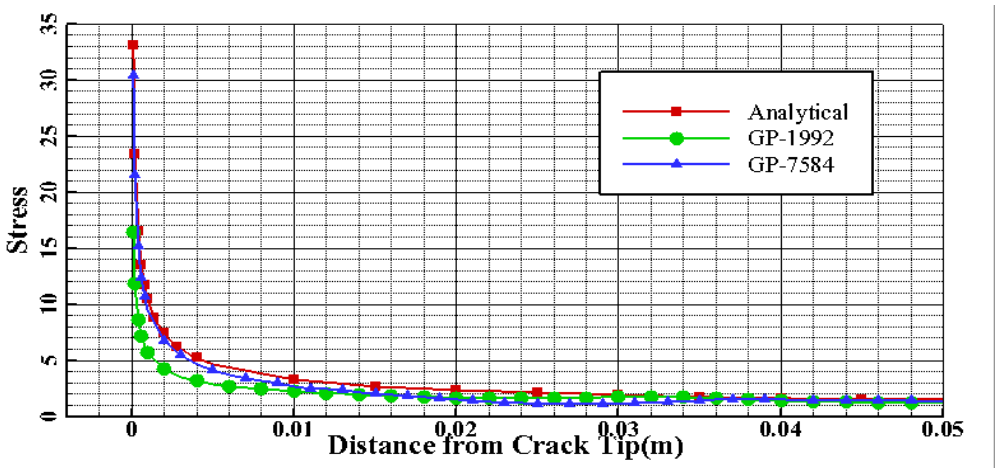

Fig. 9 - The variation in stress along the crack tip for 865 nodes and different numbers of Gauss points

b. Center-Cracked Plate

As demonstrated in Fig.12, a plate was investigated with dimensions of 2×2 m and a central crack subjected to the tensile stress of $\sigma = 1^{Mpa}$ in the lower and upper edges. The length of the central crack was equal to 0.4 m. For the symmetry shown in Fig. 8(b), a second plate with regular nodal arrangement was analyzed. For comparing the results of the Stress Intensity Factors(SIFs) obtained from the proposed extended element-free Galerkin method and meshless method based on Shepard function and Partition of Unity introduced by Cai et al., elasticity coefficient and Poisson coefficient were chosen as $E = 3\times10^4\ Mpa$ and $\nu = 0.25$, respectively. The correction factor C for calculation of the K_I is obtained by:

$$C = 1.00 + 0.128(a/W) - 0.288(a/W)^2 + 1.523(a/W)^3 \qquad (42)$$

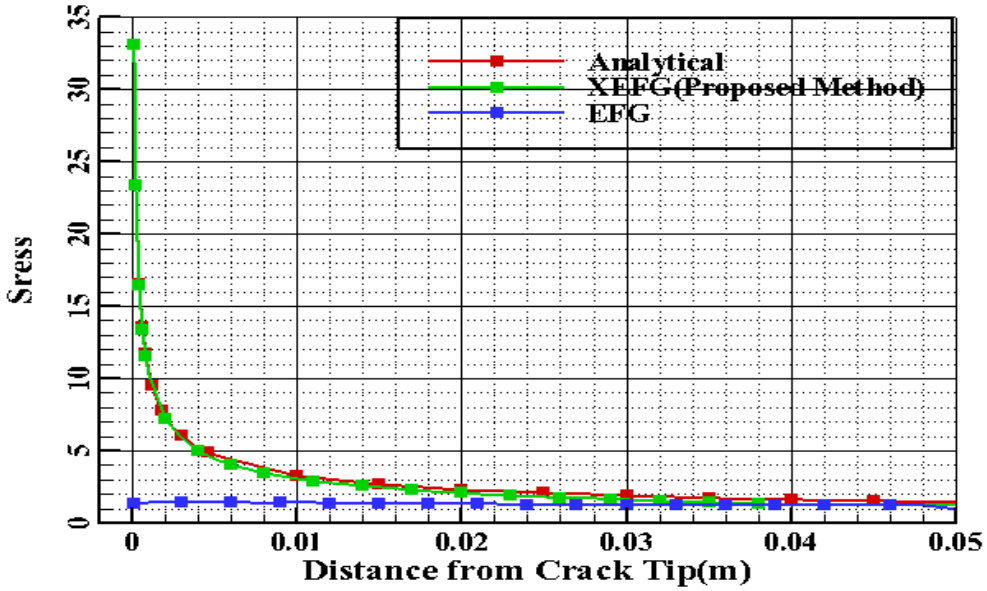

Fig. 10 - Comparison of stress variations along the crack tip for XEFG, EFG, and analytical methods

Table 2 - K_I and error values obtained relative to the analytical values

865		499		233		
Error	**$K_{I\text{-}XEFG}$**	**Error**	**$K_{I\text{-}XEFG}$**	**Error**	**$K_{I\text{-}XEFG}$**	
6.19	0.90479	3.76	0.86151	-	-	7584
5.91	0.87934	2.92	0.85454	1.36	0.84159	4338
20.65	1.0017	-	-	7.65	0.89378	1992
-	-	8.15	0.76259	12.22	0.72878	1410

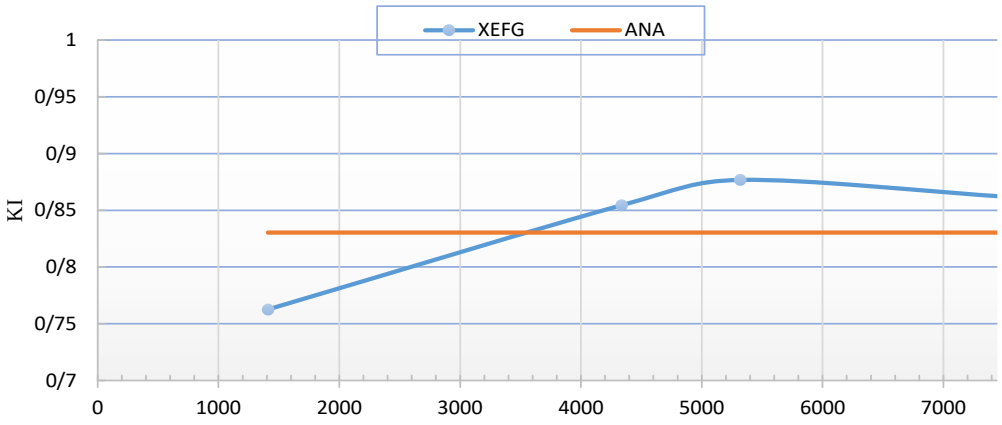

Fig. 11 - Diagram of K_I values obtained by the XEFG method for 499 nodes relative to the analytical values

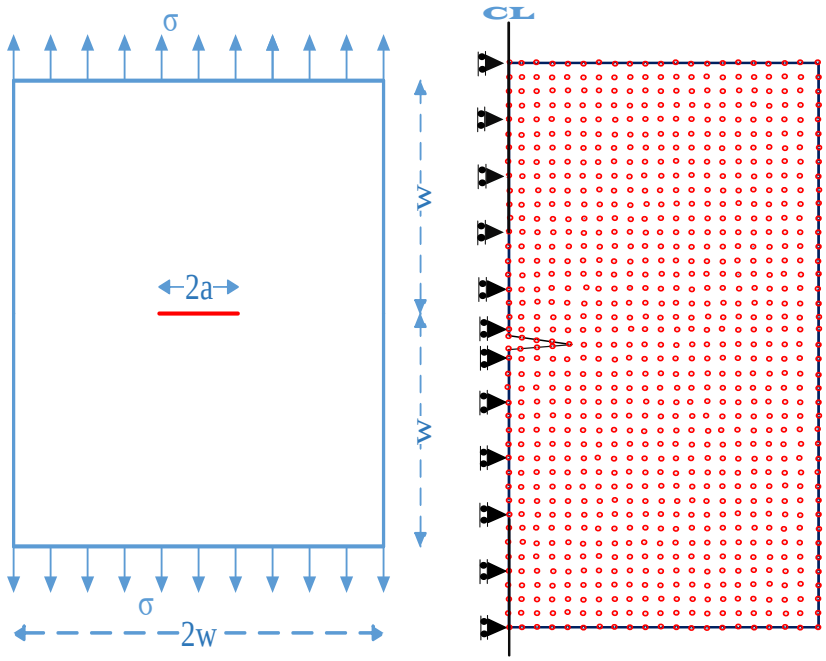

Fig. 12 - (a) Plate with a central crack under uniform tension (b) Node arrangement

Fig.13 shows the stress results along the crack tip for enrichment and non-enrichment conditions. It was observed that enrichment of the basis function greatly improves the accuracy of stress values for the same number of nodes, and the results had a good accuracy compared to the analytical results. It is very effective to select the number of Gauss points with respect to the nodal points in order to increase the accuracy of the stress values around the crack. (Fig.14) Table 3 describes the values of the stress concentration factors for the proposed extended element-free Galerkin method, the MSPU method introduced by Cai et al., and the analytical values. The results of the XEFG method had a proper accuracy for the node numbers of 865 and 499 and the increase in the number of a node resulted in more accurate results. However, the arrangement of nodes in the proposed method was regular and in the MSPU method, it was irregular with node density in the domain of cracks.

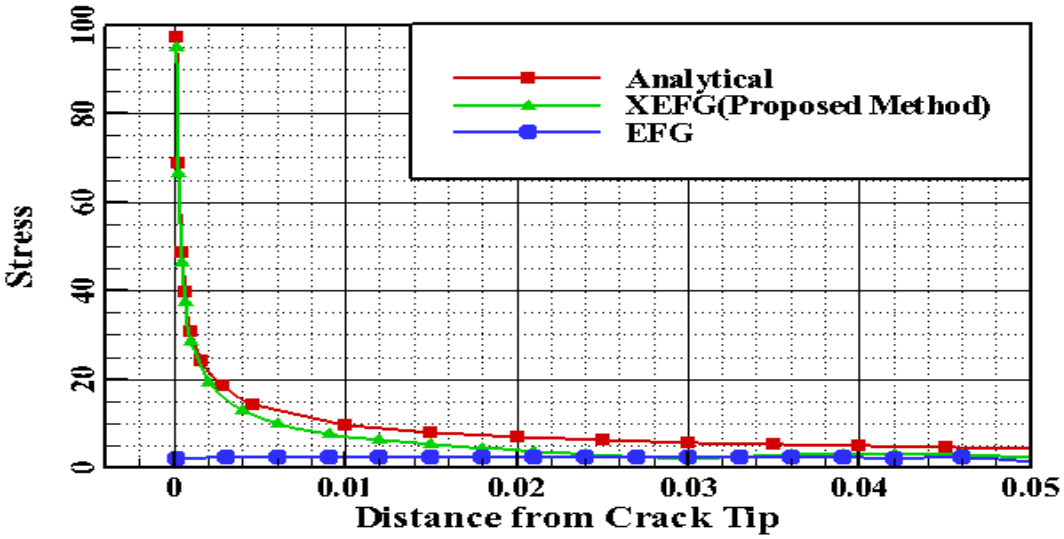

Fig. 13 - The variation in stress along the crack tip for 865 nodes and different numbers of Gauss points

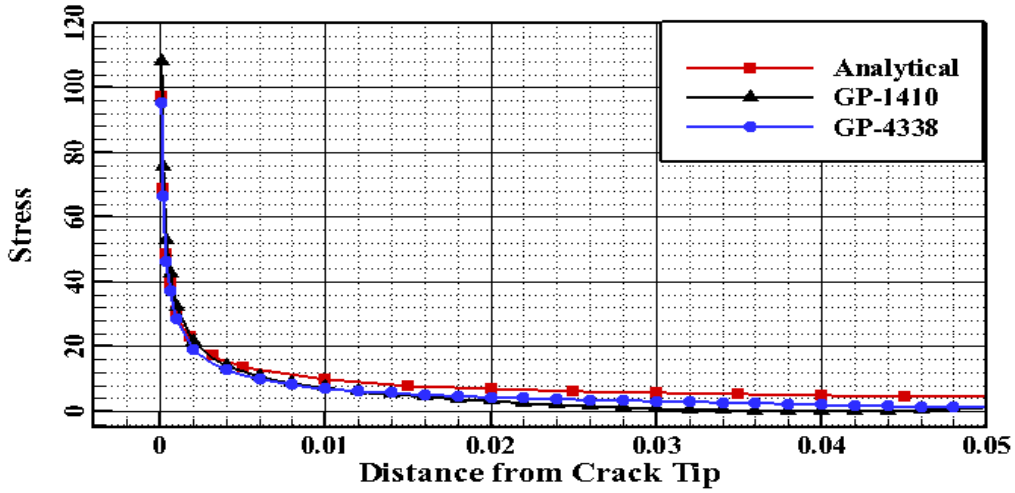

Fig. 14 - Comparison of stress variations along the crack tip for XEFG, EFG, and analytical methods

Table 3 - SIFs $Mpa\sqrt{m}$ of the plate with a central crack

Method	XEFG	XEFG	MSPU	Analytical
Node	499	865	2333	------
K_I	2.0904	2.4323	2.4202	2.4404

SIFs were determined using the domain form of the J-integral shown in Figs.15-16. The results are related to the node numbers of 865 and 499. The J-integral was theoretically independent of domain, but there was an oscillation in the results. As can be seen, the results are of good accuracy in the paths with the lengths of 0.1a and 0.2a.

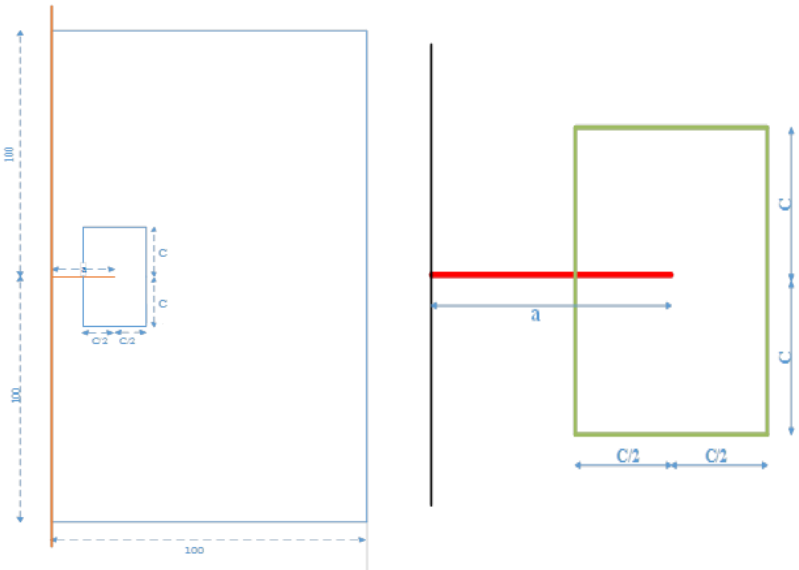

Fig. 15 - Domain for calculating the J-integral

The results of the stress concentration factor in different paths had lower variation for the node number of 865 than the node number of 499 showing that the stress distribution has a reasonable smoothness around the crack following the increase in the node number. As for the computational time (total CPU time) comparison for different nodal distributions are illustrated in Table 4.

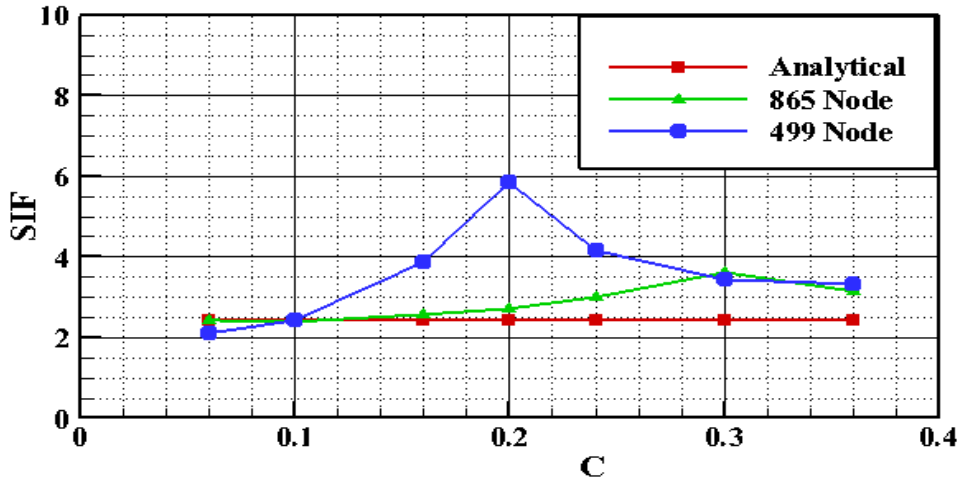

Fig. 16 - Effects of changes in the dimensions of the integration domain on K_I

Table 4 - The computational time (total CPU time) comparison for number of different nodal.

Node	233	499	865
Time(sec)	83.03	173.05	292.91

8. Conclusion

The phenomenon of structural cracking is among the most important factors in the structural failure, which is also one of the special challenges and difficulties of the engineers in numerical The phenomenon of structural cracking is among the most important factors in the structural failure, which is also one of the special challenges and difficulties of the engineers in numerical modeling. Although, the FEM has a good ability to model the cracks, the use of the shape functions, and high cost of meshing creates some limitations in the analysis of such problems. Over the past few decades, numerous research has been carried out on the mesh-free methods in solving differential equations and problems involving the cracks. The EFG method is one of the numerical methods used for solving the structural problems. This method has some advantages including the accuracy, simplicity, and low cost of calculation eliminating many difficulties of the mesh-based methods. Thus, in the current research, this method was used to analyze the problems of elastic fracture mechanics including the plates subjected to tension with edge and double and centeral cracks. A set of nodes with regular arrangement was used on the surface of the model to discretize the problems. Two approaches were applied as the main challenge in the computational mechanism in order to correctly calculate the stress concentration factor and stress around the crack tip. Firstly, the basis functions were enriched by adding the components of the near-tip displacement field for total nodes. The simplicity and convenience of use in this method is considered a feature and advantage of the proposed method. Then, the diffraction criterion technique, as one of the most efficient methods for introducing the cracks in the mesh-free method was utilized in order to apply the discontinuities caused by the presence of cracks. It should be noted that, the J-integral method was also used to calculate the stress concentration factor. The results regarding the calculation of J-integrals showed that in the rectangular path, the path width was suitably selected about 0.1 - 0.2 of the crack length. The results of the stress field analysis for the edge-cracked, double-cracked, and center-cracked plates showed that the singularity phenomenon of the stress at the crack tip can be seen very obviously by the predicted method and the stress in the crack was acceptable compared to the theoretical results. Clearly, the results showed that increasing the number of nodes is very effective in the accuracy of the results, and selection of the number of Gauss points proportional to the node number is also important. It should be noted that, increasing the number of nodes and Gauss points leads to an increase in the computational cost. Thus, in the future studies, it is suggested to investigate on the concept of cohesive crack to simulate the nonlinear behavior of the materials in the fracture process zone, which may be effective in the accuracy of the results.

Acknowledgement

The author would like to acknowledge the Faculty of Civil Engineering, Babol Noshirvani University of Technology, Babol, Iran.

Reference:

[1] R. A. Gingold and J. J. Monaghan, (1977). Smoothed particle hydrodynamics: theory and application to non-spherical stars, *Mon. Not. R. Astron. Soc.*, vol. 181, no. 3, pp. 375–389, doi: 10.1093/mnras/181.3.375.

[2] T. Belytschko, Y. Y. Lu, and L. Gu, (194). Element-free Galerkin methods. *Int. J. Numer. Methods Eng.*, vol. 37, no. 2, pp. 229–256 , doi: 10.1002/nme.1620370205.

[3] W. K. Liu, S. Jun, and Y. F. Zhang, (1995). Reproducing kernel particle methods, *Int. J. Numer. Methods Fluids*, vol. 20, no. 8-9, pp. 1081–1106, doi: 10.1002/fld.1650200824.

[4] E. Onate, S. Idelsohn. C. Zienkiewicz, and R. L. Taylor, (1996). A Finite Point Method In Computational Mechanics. Applications To Convective Transport and Fluid Flow, *Int. J. Numer. Methods Eng.*, vol. 39, no. 22, pp. 3839–3866, Nov. doi: 10.1002/(SICI)1097-0207(19961130)39:22<3839::AID-NME27>3.0.CO;2-R.

[5] T. Liszka, C. Duarte, and W. Tworzydlo,(1996) . hp-Meshless cloud method, (1996). *Comput. Methods Appl. Mech. Eng.*, vol. 139, no. 263–288.

[6] S. . Long, Shuyao and Atluri, (2002). A meshless local Petrov-Galerkin method for solving the bending problem of a thin plate. *Comput. Model. Eng. Sci.*, vol. 3, pp. 53–64.

[7] S. N. Atluri, H.-G. Kim, and J. Y. Cho. (1999). A critical assessment of the truly Meshless Local Petrov-Galerkin (MLPG), and Local Boundary Integral Equation (LBIE) methods," *Comput. Mech.*, vol. 24, no. 5, pp. 348–372. doi: 10.1007/s004660050457.

[8] N. R. Aluru and G. Li. (2001) .Finite cloud method: a true meshless technique based on a fixed reproducing kernel approximation. " *Int. J. Numer. Methods Eng.*, vol. 50, no. 10, pp. 2373–2410. doi: 10.1002/nme.124.

[9] A. R. Firoozjaee and M. H. Afshar. (2008). Discrete least squares meshless method with sampling points for the solution of elliptic partial differential equations," *Eng. Anal. Bound. Elem.*, vol. 33, no. 1, pp. 83–92. doi: https://doi.org/10.1016/j.enganabound.2008.03.004.

[10] M. H. Afshar and A. R. Firoozjaee. (2010). Adaptive simulation of two dimensional hyperbolic problems by Collocated Discrete Least Squares Meshless method. *Comput. Fluids*, vol. 39, no. 10, pp. 2030–2039, doi: https://doi.org/10.1016/j.compfluid.2010.07.005.

[11] B. Nayroles, G. Touzot, and P. Villon. (1992). Generalizing the finite element method: Diffuse approximation and diffuse elements. *Comput. Mech.*, vol. 10, no. 5, pp. 307–318. doi: 10.1007/BF00364252.

[12] R. S. Barsoum. (1976). On the use of isoparametric finite elements in linear fracture mechanics. *Int. J. Numer. Methods Eng.*, vol. 10, no. 1, pp. 25–37. doi: 10.1002/nme.1620100103.

[13] E. F. Rybicki and M. F. Kanninen. (1977). A finite element calculation of stress intensity factors by a modified crack closure integral. *Eng. Fract. Mech.*, vol. 9, no. 4, pp. 931–938. doi: https://doi.org/10.1016/0013-7944(77)90013-3.

[14] R. S. Barsoum. (1977). Triangular quarter-point elements as elastic and perfectly-plastic crack tip elements. *Int. J. Numer. Methods Eng.*, vol. 11, no. 1, pp. 85–98. doi: 10.1002/nme.1620110109.

[15] T. Belytschko and T. Black. (1999). Elastic crack growth in finite elements with minimal remeshing. *Int. J. Numer. Methods Eng.*, vol. 45, no. 5, pp. 601–620, Jun. doi: 10.1002/(SICI)1097-0207(19990620)45:5<601::AID-NME598>3.0.CO;2-S.

[16] G. R. Liu, T. Nguyen-Thoi, H. Nguyen-Xuan, and K. Y. Lam. (2009). A node-based smoothed finite element method (NS-FEM) for upper bound solutions to solid mechanics problems. *Comput. Struct.*, vol. 87, no. 1, pp. 14–26. doi: https://doi.org/10.1016/j.compstruc.2008.09.003.

[17] A. [Kamali Yazdi] and A. Shooshtari. (2015). A new two-dimensional cracked finite element for fracture mechanics. *Eng. Fract. Mech.*, vol. 135, pp. 17–33. doi: https://doi.org/10.1016/j.engfracmech.2015.01.013.

[18] S. K. Chan, I. S. Tuba, and W. K. Wilson. (1970). On the finite element method in linear fracture mechanics. *Eng. Fract. Mech.*, vol. 2, no. 1, pp. 1–17, 1970, doi: https://doi.org/10.1016/0013-7944(70)90026-3.

[19] V. B. Watwood. (1970). The finite element method for prediction of crack behavior. *Nucl. Eng. Des.*, vol. 11, no. 2, pp. 323–332. doi: https://doi.org/10.1016/0029-5493(70)90155-X.

[20] R. D. Henshell and K. G. Shaw. (1975). Crack tip finite elements are unnecessary. *Int. J. Numer. Methods Eng.*, vol. 9, no. 3, pp. 495–507. doi: 10.1002/nme.1620090302.

[21] J. C. Gálvez, J. Planas, J. M. Sancho, E. Reyes, D. A. Cendón, and M. J. Casati. (2013). An embedded cohesive crack model for finite element analysis of quasi-brittle materials. *Eng. Fract. Mech.*, vol. 109, pp. 369–386. doi: https://doi.org/10.1016/j.engfracmech.2012.08.021.

[22] N. Sukumar, N. Moës, B. Moran, and T. Belytschko. (2000). Extended finite element method for three-dimensional crack modelling. *Int. J. Numer. Methods Eng.*, vol. 48, no. 11, pp. 1549–1570. doi: 10.1002/1097-0207(20000820)48:11<1549::AID-NME955>3.0.CO;2-A.

[23] J. Chessa, P. Smolinski, and T. Belytschko. (2002). The extended finite element method (XFEM) for solidification problems. *Int. J. Numer. Methods Eng.*, vol. 53, no. 8, pp. 1959–1977. doi: 10.1002/nme.386.

[24] N. Moës and T. Belytschko.(2002). Extended finite element method for cohesive crack growth. *Eng. Fract. Mech.*, vol. 69, no. 7, pp. 813–833. doi: https://doi.org/10.1016/S0013-7944(01)00128-X.

[25] J. Lee and H. Gao. (1995). A hybrid finite element analysis of interface cracks. *Int. J. Numer. Methods Eng.*, vol. 38, no. 14, pp. 2465–2482. doi: 10.1002/nme.1620381410.

[26] S. N. Atluri, A. S. Kobayashi, and M. Nakagaki. (1975). Fracture Mechanics Application of an Assumed Displacement Hybrid Finite Element Procedure. *AIAA J.*, vol. 13, no. 6, pp. 734–739. doi: 10.2514/3.60429.

[27] J. M. Melenk and I. Babuška. (1996). *The Partition of Unity Finite Element Method: Basic Theory and Applications*. Texas Institute for Computational and Applied Mathematics, University of Texas at Austin.

[28] M. Fleming, Y. A. Chu, B. Moran, and T. Belytschko. (1997). Enriched Element-Free Galerkin Methods for Crack Tip Fields. *Int. J. Numer. Methods Eng.*, vol. 40, no. 8, pp. 1483–1504. doi: 10.1002/(SICI)1097-0207(19970430)40:8<1483::AID-NME123>3.0.CO;2-6.

[29] W. Ma, G. Liu, and H. Ma. (2019). A smoothed enriched meshfree Galerkin method with two-level nesting triangular sub-domains for stress intensity factors at crack tips. Theor. Appl. Fract. Mech., vol. 101, pp. 279–293. doi: https://doi.org/10.1016/j.tafmec. 2019.03.011.

[30] F. Liaghat, M. R. Hematiyan, A. Khosravifard, and T. Rabczuk. (2019). A robust meshfree method for analysis of cohesive crack propagation problems," *Theor. Appl. Fract. Mech.*, vol. 104, p. 102328. doi: https://doi.org/10.1016/j.tafmec.2019.102328.

[31] T. Belytschko, Y. Y. Lu, and L. Gu. (1995). Crack propagation by element-free Galerkin methods. *Eng. Fract. Mech.*, vol. 51, no. 2, pp. 295–315. doi: https://doi.org/10.1016/0013-7944(94)00153-9.

[32] T. Belytschko, L. Gu, and Y. Y. Lu. (1994). Fracture and crack growth by element free Galerkin methods. *Model. Simul. Mater. Sci. Eng.*, vol. 2, no. 3A, pp. 519–534. doi: 10.1088/0965-0393/2/3a/007.

[33] N. Muthu, B. G. Falzon, S. K. Maiti, and S. Khoddam. (2014). Modified crack closure integral technique for extraction of SIFs in meshfree methods. *Finite Elem. Anal. Des.*, vol. 78, pp. 25–39. doi: https://doi.org 10.1016/j.finel.2013.09.005.

[34] V. Kumar and R. Drathi. (2014). A meshless Cracking Particles Approach for ductile fracture. *KSCE J. Civ. Eng.*, vol. 18, no. 1, pp. 238–248. doi: 10.1007/s12205-014-0164-4.

[35] Y. Cai, L. Han, L. Tian, and L. Zhang. (2016). Meshless method based on Shepard function and partition of unity for two-dimensional crack problems. *Eng. Anal. Bound. Elem.*, vol. 65, pp. 126–135. doi: https://doi.org/10.1016/j.enganabound.2016.01.009.

[36] W. Ma, G. Liu, and W. Wang. (2020). A coupled extended meshfree–smoothed meshfree method for crack growth simulation. Theor. Appl. Fract. Mech., vol. 107, p. 102572. doi: https://doi.org/10.1016/ j.tafmec.2020.102572.

[37] X. Zhuang, Y. Cai, and C. Augarde. (2014). A meshless sub-region radial point interpolation method for accurate calculation of crack tip fields. *Theor. Appl. Fract. Mech.*, vol. 69, pp. 118–125. doi: https://doi.org/10.1016/j.tafmec.2013.12.003.

[38] S. C. Li, S. C. Li, and Y. M. Cheng. (2005). Enriched meshless manifold method for two-dimensional crack modeling. *Theor. Appl. Fract. Mech.*, vol. 44, no. 3, pp. 234–248. doi: https://doi.org/10.1016/ j.tafmec.2005.09.002.

[39] S. N. S. Mortazavi, A. Ince. (2020). An artificial neural network modeling approach for short and long fatigue crack propagation. Computational Materials Science,Volume 185.doi :https://doi.org/10.1016/j.commatsci. 2020.109962

[40] D Gope, PC Gope, A Thakur, A Yadav. (2015). Application of artificial neural network for predictingcrack growth direction in multiple cracks geometry. Applied Soft ComputingVolume 30. Pages 514-528 https://doi.org/ 10.1016/j.asoc.2015.02.003Get rights and content

[41] Q Yang, G Li, W Mu, G Liu, H Sun. (2020). Identification of crack length and angle at the center weld seam of offshore platforms using a neural network approach. J. Mar. Sci. Eng. 2020, 8(1), 40; https://doi.org/ 10.3390/jmse8010040

[42] E. E. Gdoutos, *Fracture Mechanics: An Introduction*. Springer Netherlands, 2006.

[43] G. R. Liu, *Mesh free methods: Moving beyond the finite element method*. 2002.